

Computer-Assisted Discrimination Among Malignant Lymphomas and Leukemia Using Immunophenotyping, Intelligent Image Repositories, and Telemicroscopy

David J. Foran, *Member, IEEE*, Dorin Comaniciu, *Member, IEEE*, Peter Meer, *Senior Member, IEEE*, and Lauri A. Goodell

Abstract—The process of discriminating among pathologies involving peripheral blood, bone marrow, and lymph node has traditionally begun with subjective morphological assessment of cellular materials viewed using light microscopy. The subtle visible differences exhibited by some malignant lymphomas and leukemia, however, give rise to a significant number of false negatives during microscopic evaluation by medical technologists. We have developed a distributed, clinical decision support prototype for distinguishing among hematologic malignancies. The system consists of two major components, a distributed telemicroscopy system and an intelligent image repository. The hybrid system enables individuals located at disparate clinical and research sites to engage in interactive consultation and to obtain computer-assisted decision support. Software, written in JAVA, allows primary users to control the specimen stage, objective lens, light levels, and focus of a robotic microscope remotely while a digital representation of the specimen is continuously broadcast to all session participants. Primary user status can be passed as a token. The system features shared graphical pointers, text messaging capability, and automated database management. Search engines for the database allow one to automatically identify and retrieve images, diagnoses, and correlated clinical data of cases from a “gold standard” database which exhibit spectral and spatial profiles which are most similar to a given query image. The system suggests the most likely diagnosis based on majority logic of the retrieved cases. The system was used to discriminate among three lymphoproliferative disorders and healthy cells. The system provided the correct classification in more than 83% of the cases studied. System performance was evaluated using rigorous statistical assessment and by comparison with human observers.

Manuscript received September 1999; revised January 2000. This work was supported by an R&D Excellence Award from the New Jersey Commission on Science and Technology. D. J. Foran and L. A. Goodell were supported by the Whitaker Foundation through Grant 98-0202. P. Meer and D. Comaniciu were supported by the National Science Foundation through Grants IRI-9530546 and IRI 9618854.

D. J. Foran is with the Center for Biomedical Imaging & Informatics, UMDNJ-Robert Wood Johnson Medical School, Piscataway, NJ 08854 USA.

D. Comaniciu is with the Department of Imaging & Visualization, Siemens Corporate Research, Princeton, NJ 08540 USA.

P. Meer is with the Department of Computer and Electrical Engineering, Rutgers University, Piscataway, NJ 08854 USA.

L. A. Goodell is with the Department of Pathology & Laboratory Medicine, UMDNJ-Robert Wood Johnson Medical School, Piscataway, NJ 08854 USA.

Publisher Item Identifier S 1089-7771(00)03949-2.

I. INTRODUCTION

Clinical Background

A differential diagnosis affects how aggressively patients are treated, which medications are appropriate, and what levels of risk are justified. As new treatments become available, each targeting specific clinical profiles, it has become increasingly important to distinguish among subclasses of pathologies [1]. Peripheral blood smears are routinely screened and constituent cellular material differentiated based upon traditional morphological characteristics; however, the subtle visible differences exhibited by some malignant lymphomas and leukemia give rise to a significant number of false negatives during microscopic evaluation by medical technologists.

Mantle cell lymphoma (MCL) is a recently described entity, which is often misdiagnosed as chronic lymphocytic leukemia (CLL) or as follicular center cell lymphoma (FCC). The significance of timely, accurate diagnosis of MCL is of extreme importance since it has a more aggressive clinical course than CLL or FCC. MCL is considered an intermediate grade lymphoma with a 3–5-yr median survival rate [5], [2], [3]. Although there is an entire spectrum of presentations for this disorder, the classic morphologic description is a monotonous proliferation of small to medium sized lymphoid cells with scant cytoplasm, variably irregular and indented nuclei (sometimes round), dispersed chromatin, inconspicuous nucleoli, and scant cytoplasm. The immunophenotype is CD5 positive B cells which are FMC7 antigen positive with moderately bright surface membrane immunoglobulin light chain expression, CD23 negative, and usually CD10 negative [5]. The lack of CD23 expression differentiates this entity from typical CLL. Confusion between these two can arise when CLL loses CD23 during disease progression.

Chronic lymphocytic leukemia (CLL) is the most frequent leukemia in Western countries. It is typically considered indolent and incurable but can sometimes progress to a more aggressive disease [5], [6]. The classic morphologic description of typical CLL cells is small lymphocytes containing round nuclei with coarsely condensed chromatin and scant cytoplasm. The immunophenotype for CLL is CD5 positive antigen expression on B cells with CD23 antigen positivity, low-density surface membrane immunoglobulin restricted light chain positivity, and CD10 negative [5]–[8]. This immunophenotype is considered to be the diagnostic gold standard for CLL. Evolution to

an atypical CLL is associated with deviations in immunophenotype. Such changes can lead to a misdiagnosis as mantle cell lymphoma [6], [8].

Follicular center cell lymphoma (FCC) is considered a low-grade lymphoma within the Working Formulation. The classic morphologic description of FCC cells is small to medium sized lymphoid cells with markedly angulated and cleaved nuclei, coarse chromatin, inconspicuous nucleoli, and scant cytoplasm. The classic immunophenotype consists of CD5 negative B cells with positive CD10 expression and moderately bright expression of surface membrane immunoglobulin light chain expression [5]. FCC has an indolent course and is usually incurable. The disease often progresses to an aggressive high-grade large-cell lymphoma. The median survival is 6–8 years [5].

Recent literature ascribes much of the difficulty in rendering consistent diagnoses to subjective impressions of observers and shows that, when morphologic cell classification is based upon computer-aided analysis, objectivity and reproducibility improve [10]–[13]. One might use subtle changes in measurable parameters to discover novel diagnostic clues, which are not normally apparent by human visual inspection. We have divided the problem of computer-assisted diagnosis into parts, one part focusing on those aspects in which computers are most adept, such as gathering data and performing objective low-level processing of information, and one part concentrating on those aspects in which humans are best suited, such as complex reasoning, consideration of interdependencies among findings, on high level abstractions, and on rendering clinical decisions. The prototype that we have developed consists of a distributed telemicroscopy system operating in concert with an intelligent image database. The system enables consulting physicians and scientists to engage in interactive telemicroscopy sessions and to automatically search through databases of consensus-graded medical cases based upon the visual content of constituent pathology image records in order to obtain reliable decision support in detecting and discriminating among hematologic malignancies.

II. METHODS

A. Imaging

Immunophenotyping by flow cytometry was used to confirm the diagnosis for 19 lymphoproliferative cases [5 mantle cell lymphoma (MCL), 5 chronic lymphocytic leukemia (CLL), 4 follicular center cell lymphoma (FCC)] and 5 normal (benign) cases at the Division of Hematopathology, Robert Wood Johnson University Hospital, New Brunswick, NJ. Wright stained peripheral blood smears were prepared for each specimen using standard methods of air drying, fixation with methanol, and staining with Wright Giemsa solution. Stained specimens were subsequently examined by a certified hematopathologist during the course of several sessions using a Leica microscope, 40x planachromatic objective while lymphoid cells and benign lymphocytes were identified, digitized, and stored to disk in 24-bit TIFF format using interactive software developed in C++. The imaging components of the system consist of an Intel-based workstation interfaced

to a high-resolution 3-chip Olympus (OLY-750) color video camera and a Coreco Oculus data acquisition board. The image database used in the study consisted of 66 MCL, 98 CLL, 38 FCC, and 59 benign cells.

B. Segmentation and Shape Analysis

Segmentation of images was accomplished by mapping red, green, and blue intensity values of the imaged specimens into $L^*u^*v^*$ color space and utilizing the fast nonparametric clustering method developed by Comaniciu and Meer [14]. The x, y coordinates corresponding to the outer boundary of delineated biological structures within the segmented images served as input for shape analysis. To avert burdening the recognition component of the system, the shape analysis module was developed using a global descriptor in the lowest possible dimensional space. While statistical shape theory in general tends to focus on landmark-based approaches [15], such strategies would be extremely unreliable in our studies since we deal with coarsely digitized curves. Since cells in the digitized specimens exhibit arbitrary locations and orientations, we sought feature descriptors which were invariant to translation and rotation. While there are a host of feature measurements that might have been considered for use in these studies [16]–[19], we chose to utilize elliptic Fourier descriptors to develop the prototype system. Fourier invariants have recently proved to be superior to methods based on autoregression models [20]. Elliptic Fourier descriptors [21] of a closed curve are given by the following equations:

$$\begin{aligned} a_n &= \frac{T}{2n^2\pi^2} \sum_{i=1}^m \frac{\Delta x_i}{\Delta t_i} \left[\cos\left(\frac{2n\pi t_i}{T}\right) - \cos\left(\frac{2n\pi t_{i-1}}{T}\right) \right] \\ b_n &= \frac{T}{2n^2\pi^2} \sum_{i=1}^m \frac{\Delta x_i}{\Delta t_i} \left[\sin\left(\frac{2n\pi t_i}{T}\right) - \sin\left(\frac{2n\pi t_{i-1}}{T}\right) \right] \\ c_n &= \frac{T}{2n^2\pi^2} \sum_{i=1}^m \frac{\Delta y_i}{\Delta t_i} \left[\cos\left(\frac{2n\pi t_i}{T}\right) - \cos\left(\frac{2n\pi t_{i-1}}{T}\right) \right] \\ d_n &= \frac{T}{2n^2\pi^2} \sum_{i=1}^m \frac{\Delta y_i}{\Delta t_i} \left[\sin\left(\frac{2n\pi t_i}{T}\right) - \sin\left(\frac{2n\pi t_{i-1}}{T}\right) \right] \end{aligned}$$

where

$$\begin{aligned} \Delta x_i &= (x_i - x_{i-1}) \\ \Delta y_i &= (y_i - y_{i-1}), \\ \Delta t_i &= \sqrt{(\Delta x_i)^2 + (\Delta y_i)^2} \\ t_i &= \sum_{j=1}^i \Delta t_j \\ T &= \sum_{i=1}^m \Delta t_i \end{aligned}$$

with the phase shift from the first major axis given by

$$\theta_1 = \frac{1}{2} \left[\frac{2(a_1 b_1 + c_1 d_1)}{a_1^2 + b_1^2 + c_1^2 + d_1^2} \right].$$

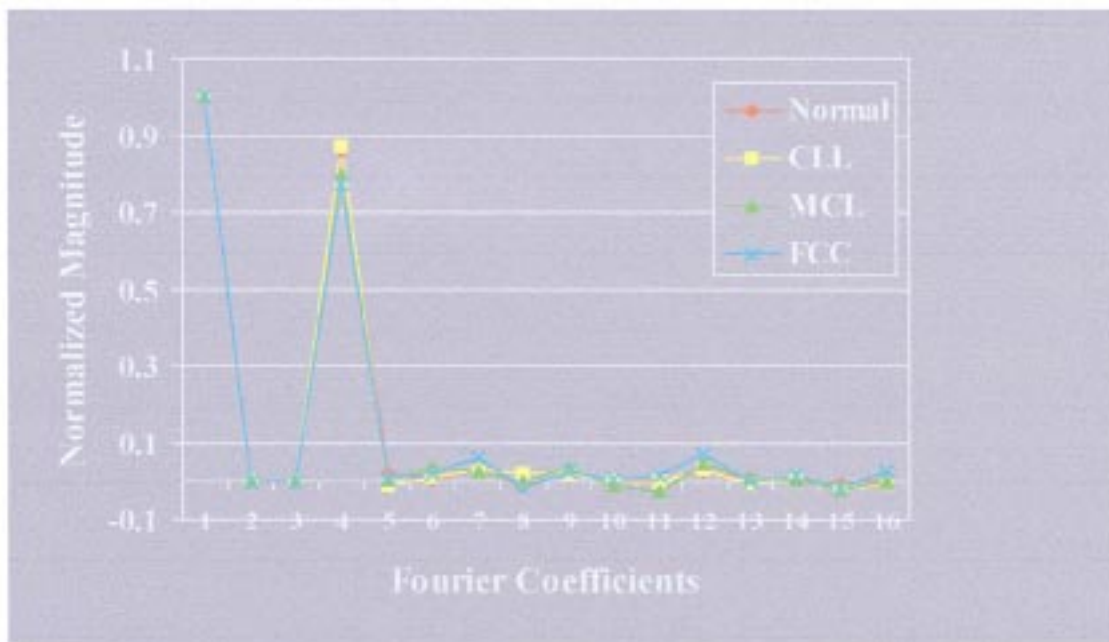


Fig. 1. First 16 Fourier coefficients for representative normal, CLL, MCL, and FCC cells.

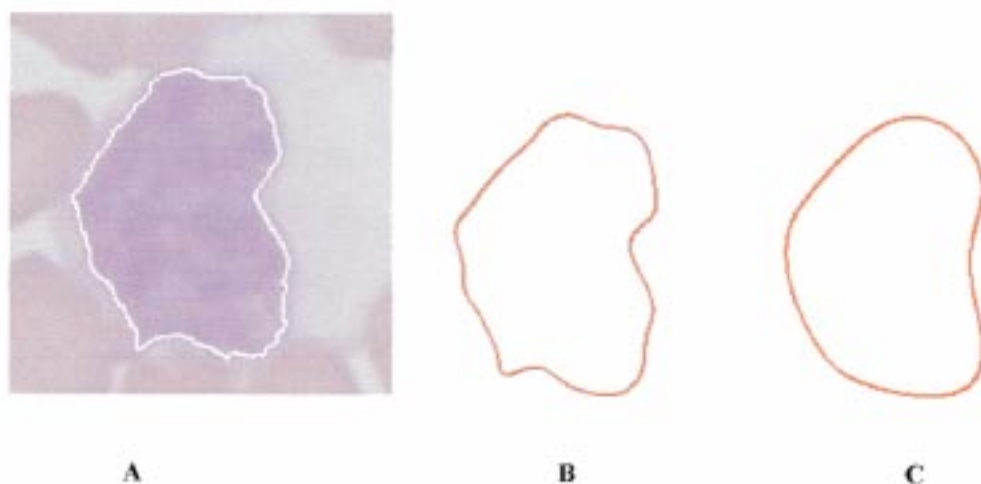


Fig. 2. Representation of a closed contour by elliptic Fourier descriptors. (a) Input. (b) Series truncated at 16 harmonics. (c) Series truncated to four harmonics.

Fig. 1 shows the first 16 Fourier coefficients for representative normal, CLL, MCL, and FCC cells.

Elliptic Fourier descriptors were apparently overlooked in the recent revival of techniques for image content-based indexing, in spite of having the advantage of preserving topology when the Fourier series are truncated (Fig. 2).

While the system automatically generates the first 16 harmonics (64 coefficients) for each delineated contour, there appears to be no significant loss in performance when truncating to 10 harmonics (40 coefficients). Consequently, we compare query contours with reference contours in the database by computing the Euclidean distance between the corresponding 40-dimensional vectors of Fourier invariants using the following equation:

$$D_1 = \sqrt{(f_{\text{query}} - f_{\text{reference}})^T (f_{\text{query}} - f_{\text{reference}})}.$$

C. Multiresolution Texture

Traditionally, discrimination among lymphoproliferative disorders depends upon qualitative visual descriptions of cellular components such as graininess, chromatin pattern, and prominence of nucleoli. In recognition of this fact, the algorithms include metrics which provide objective measures of the texture of the cellular components. The texture assessment module is based on the multiscale simultaneous autoregressive (MRSAR) model [22]. It is a second-order noncausal model described by five parameters at each resolution level. The algorithm applies a symmetric MRSAR model to the L^* component of $L^*u^*v^*$ image data. The pixel value $L^*(x)$ at any location x is assumed to linearly depend upon the neighboring pixel values $L^*(y)$ and an additive independent Gaussian noise term $\varepsilon(x)$. In the equation, $L^*(x) = \mu + \sum_{y \in v} \theta(y)L^*(y) + \varepsilon(x)$, μ is the bias dependent on the mean value of L^* , v is the set of neighbors of

TABLE I
COMPUTED WEIGHTS FOR THE OVERALL DISSIMILARITY METRIC

Shape	Texture	Area
0.1140	0.5771	0.3089

the pixel at location x , and $\theta(y)$ with $y \in \mathcal{V}$ are the model parameters. Due to the symmetry of the model, $\theta(y) = \theta(-y)$ so that, for any given neighborhood, four are estimated through least squares. Thus, the model parameters and the estimation error define a 5-dimensional feature vector. The MRSAR features are computed for 5×5 , 7×7 , and 9×9 neighborhoods which give rise to a 15-dimensional multiresolution feature vector.

In order to estimate the model parameters, 21×21 overlapping windows were used. Windows were offset from one another by two pixels in both the x and y directions. A multiresolution feature vector was generated for each window. The mean vector \mathbf{t} and the covariance matrix Σ across all 441 windows constitute the MRSAR features for that nucleus.

Dissimilarity among textures was represented as the distance between multivariate distributions with known mean vectors and covariance matrices. Mahalanobis distance between MRSAR feature vectors was used to determine dissimilarity

$$D_2 = \sqrt{(t_{\text{query}} - t_{\text{reference}})^T \sum_{\text{reference}}^{-1} (t_{\text{query}} - t_{\text{reference}})}$$

where $\sum_{\text{reference}}^{-1}$ is the inverse of the covariance matrix of the covariance matrix of $t_{\text{reference}}$. For each entry in the database, $\sum_{\text{reference}}^{-1}$ was obtained and stored.

D. Area

In these studies, all specimens were digitized at the same magnification so the nuclear area was computed as the number of pixels contained within the nucleus. The dissimilarity between any two nuclei in terms of their areas is therefore

$$D_3 = \sqrt{(a_{\text{query}} - a_{\text{reference}})^2}.$$

E. Color

The nuclear color is specified as a 3-D vector in $L^*u^*v^*$ space. Since specimens were prepared and digitized at various times by various technicians, the colors of the nuclei in the database do not cluster as a function of cell class. Therefore, in the current stage of development, the color attribute was used to perform segmentation of the image, but not for discriminating among cell types.

Interactive computer algorithms were developed in JAVA to automate image processing and to generate, index, and store similarity invariant Fourier descriptors [21], measures for area, chromatic metrics, and multiresolution simultaneous autoregressive texture metrics [22] for each cell.

F. Overall Similarity Measure and Retrieval Performance

Defining an overall similarity measure for the retrieval module was relatively challenging since measurements for shape, texture, color, and area relate to different characteristics. A relatively simple solution was to express the dissimilarity as a linear combination of the normalized distances corresponding to each query attribute. Thus, for three attributes (shape, texture, and area), $D = \sum_{i=1}^3 w_i D_i$, where w_i represents the relevance of the i th attribute and $\sum_{i=1}^3 w_i = 1$. Color was not used as a query attribute in this study because of the large variation in chromatic characteristics across specimens arising from slight differences in staining times and the fact that images were digitized during various sessions.

For a given database, the optimal weights w_i were obtained by employing a downhill simplex method [23] with the objective function J . The optimization criterion is based on the retrieval matrix \mathbf{R} defined as having the element r_{jk} equal to the empirical probability of retrieval of class k images when the query belonged to class j . The objective function is the trace of the retrieval matrix expressed as

$$J = \text{trace } \mathbf{R} = \sum_{j=1}^m r_{jj}$$

where m is the number of classes.

To ensure a numerically stable optimization procedure, individual distances were normalized to the standard deviation calculated relative to the center of each class except for D_2 , which is a Mahalanobis distance and therefore has intrinsic normalization.

An iterative search was performed to find the optimal weights. Starting with all weights equal and their sum equal to 1, the objective function is computed for the first eight retrievals (closest matches) over the entire database. The weights are modified and the procedure is repeated until convergence is achieved. Table I shows the weights computed over the entire database. It corresponds to a global maximum, $J = 3.4207$, for the objective function.

The overall dissimilarity metric between two nuclei is defined as a linear combination of the normalized distances corresponding to each visual attribute. The weights are obtained off-line by optimizing the probability of correct classification over the entire database. In order to gain a realistic estimate of system performance for the prototypical system at the present stage of development, a ten-fold cross-validated classification [24] was implemented by randomized splitting of the data into 10 approximately equal test sets, each containing about 9 CLL, 3 FCC, 6 MCL, and 5 NORMAL cases. For the q th test set, its complement was used to obtain the optimal weights using the downhill simplex method [25]. The confusion matrix R_q of the resulting classifier was then computed over the q th test set

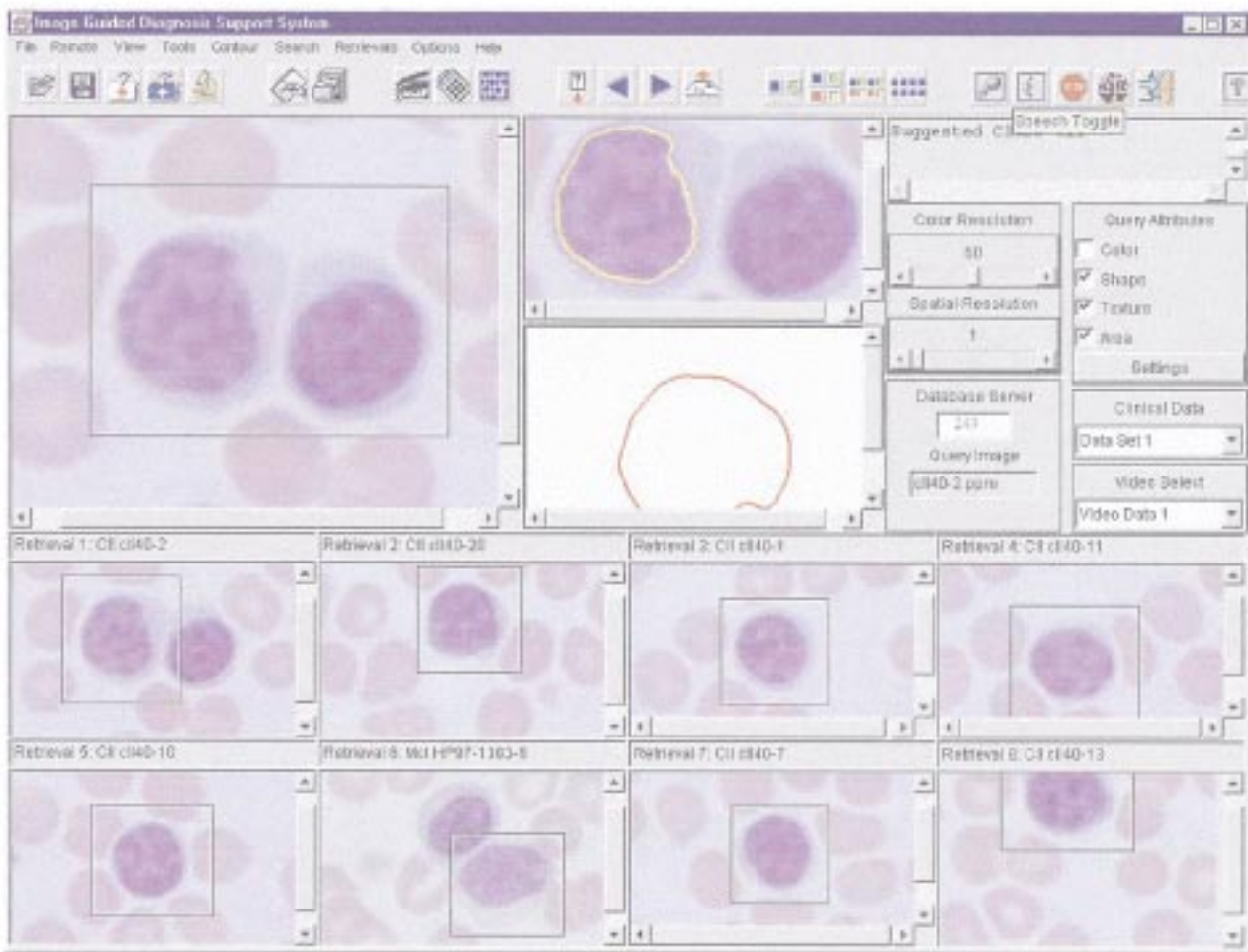


Fig. 3. The user interface of the decision support component of the system. The upper left-hand corner shows a digitized specimen containing an unidentifiable cell. The center panels show a snapshot of the system as spectral, spatial, and texture attributes of the nucleus are generated. The bottom eight panels show images that have been retrieved from the “ground truth” consensus-graded database because their profiles most closely match that of the unidentified cell. Across the top of the iconized images are three letter representations of the diagnostic class of the retrieved image.

using the first seven retrievals from the database. The class allocation of the test image was defined by the relative majority of the retrieved classes. In case of a tie, the “no decision” (NO DEC) category was incremented. The elements of the cross-validated confusion matrix were defined as the average of the 10 trials. The correct class is that of the row labels, while the allocated class is that of the column labels. The confusion matrix was computed using

$$P_{\text{cross}}(j/i) = 1/10 \sum_{q=1}^{10} P_q(j/i),$$

for $i = 1 \dots 4$ and $j = 1 \dots 5$.

G. User Interface

Fig. 3 shows a snapshot of an interactive query session as it is being conducted using the prototypical decision support approach. The system features both audio and graphic command interfaces to the search engine. A fusion agent interprets the commands, calls the appropriate method, and provides voice feedback to the user. The system currently employs a speech recognizer engine with finite-state grammar and a restricted task-specific vocabulary. Voice recognition is speaker-independent.

The decision support component of the system has been integrated with a network-based distributed telemicroscopy system. The integrated system has a client-server platform-independent architecture implemented in Java (Fig. 4).

The image server for the telemicroscopy system consists of an Intel-based Pentium II, 450-MHz computer equipped with 144 MB of RAM and Flashpoint image acquisition card. The server allows multiple users to log into the system. The first user to log into the system is designated as primary. A Java-based microcontroller was developed on the server side to process and service commands issued by the clients. The system enables primary users to remotely control the specimen stage, light levels, objective lens, and focus of a robotic microscope (Olympus AX70). The system also allows one to change the resolution and rate at which images are digitized dynamically. Primary user status can be passed as a token among participants. The system features shared graphical pointers and text messaging capability. The client component was designed to enable individuals located at remote clinical and research sites to access the database at the server site through local- and wide-area network communications.

The client I/O module allows one to load query images from local and remote microscopes and computers. The system then

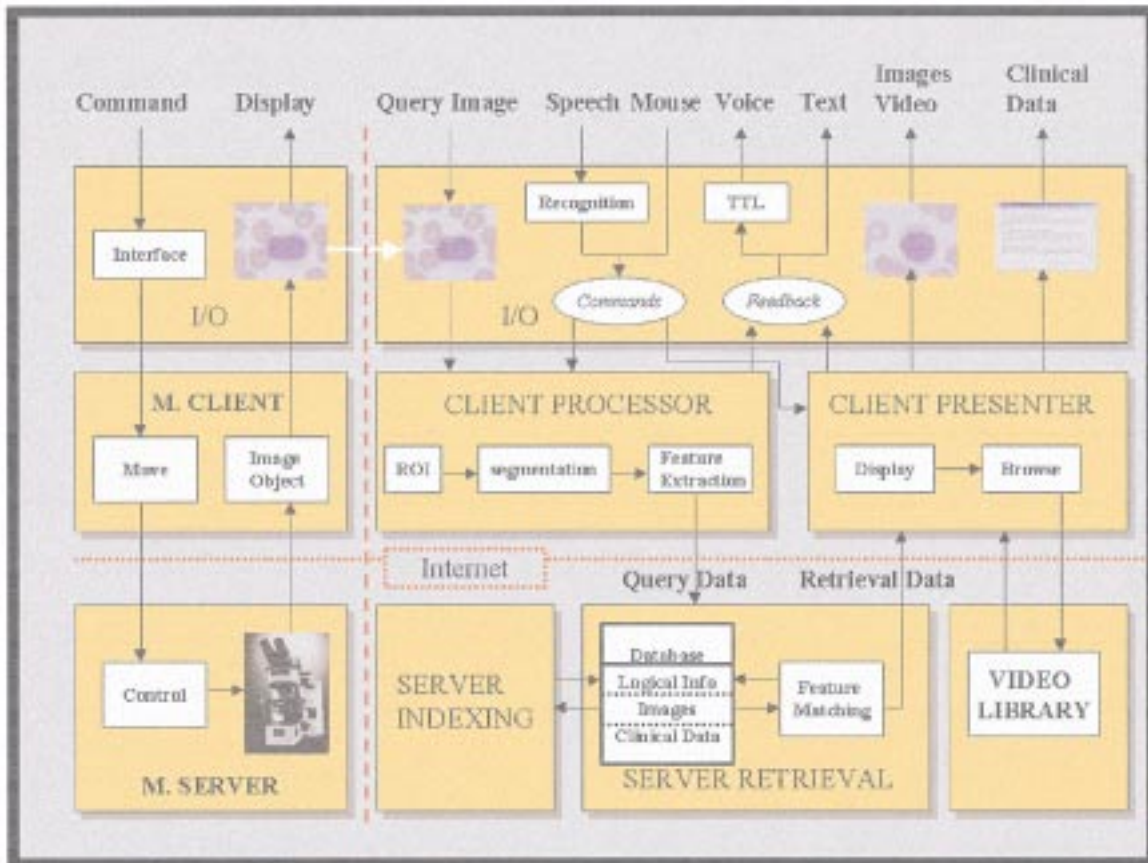


Fig. 4. Architecture of the integrated decision support and telemicroscopy system.

TABLE II
CONFUSION MATRIX: PROTOTYPE SYSTEM

	CLL	FCC	MCL	NORMAL	NO DEC
CLL	0.8389	0.200	0.0711	0.0700	0
FCC	0.0250	0.900	0.000	0.0500	0.0250
MCL	0.1357	0.0143	0.8333	0.0000	0.0167
NORMAL	0.1333	0.1200	0.000	0.7300	0.0167

performs automated color segmentation and feature extraction. A query vector is automatically generated from the feature measurements and submitted to the server. Search engines for the database automatically identify and retrieve images, diagnoses, and correlated clinical data of cases from a "gold standard" database which exhibit spectral and spatial profiles which are most similar to the query image from the undiagnosed case. Based on majority logic of the retrieved data, the client communicates the suggested classification to the user.

The indexing module of the software allows users to access both local and remote databases. When logged into a remote database, the user is categorized as belonging to either the SEARCHER, INDEXER, or INTEGRATOR/REVIEWER group. Individuals belonging to the SEARCHER group can review and process local and remote images and can query and search remote databases. Users from the INDEXER group are able to populate the databases with new images and correlated diagnoses. Members of the INTEGRATOR/REVIEWER group are able to review entries and initiate computation of weighting factors, to accommodate any new image entries. The INTE-

GRATOR/REVIEWER group can add new users to the system and assign privilege levels. All users have full accessibility to search, index, and integrate their own local databases.

III. RESULTS

The confusion matrix of the prototype is shown in Table II. The performance of the system was later compared with three classes of individuals: those in training (resident, fellow), those who perform screening of specimens for detecting abnormalities (technicians), and those responsible for rendering the differential diagnosis (e.g., certified hematopathologist). Each of the participants in the study were shown one digitized specimen at a time on a high-resolution screen with no other distractor displayed. They were asked to classify the cell as belonging to one of five classes: mantle cell lymphoma, follicular cell lymphoma, chronic lymphocytic leukemia, normal, or other. The confusion matrix showing the results of five human observers is shown in Table III.

TABLE III
CONFUSION MATRIX: HUMAN OBSERVERS

	CLL	FCC	MCL	NORMAL	NO DEC
CLL	0.5647	0.0352	0.2117	0.1764	0.0117
FCC	0.0285	0.9428	0.000	0.0285	0.0000
MCL	0.1538	0.0769	0.5538	0.1692	0.0461
NORMAL	0.1228	0.0000	0.1053	0.7543	0.0175
	Human Observer one				
	CLL	FCC	MCL	NORMAL	NO DEC
CLL	0.4000	0.0588	0.1647	0.3765	0.000
FCC	0.0000	1.000	0.000	0.000	0.0000
MCL	0.0769	0.0923	0.5538	0.1692	0.0923
NORMAL	0.0000	0.0877	0.1053	0.7719	0.0351
	Human Observer two				
	CLL	FCC	MCL	NORMAL	NO DEC
CLL	0.4941	0.0235	0.2118	0.2000	0.0471
FCC	0.000	0.8857	0.0857	0.0286	0.0000
MCL	0.4308	0.0154	0.3077	0.0308	0.2154
NORMAL	0.200	0.0364	0.1455	0.3455	0.2727
	Human Observer three				
	CLL	FCC	MCL	NORMAL	NO DEC
CLL	0.600	0.0118	0.1764	0.2118	0.0000
FCC	0.0571	0.8571	0.0000	0.0857	0.0000
MCL	0.0615	0.0923	0.5230	0.2154	0.1077
NORMAL	0.0351	0.0526	0.1053	0.8070	0.0000
	Human Observer four				
	CLL	FCC	MCL	NORMAL	NO DEC
CLL	0.7176	0.0235	0.0706	0.1529	0.0471
FCC	0.0571	0.8571	0.0000	0.0857	0.0000
MCL	0.0615	0.0615	0.3846	0.3846	0.1231
NORMAL	0.0702	0.0351	0.0000	0.8771	0.0175
	Human Observer five				

IV. DISCUSSION

Mantle cell lymphoma is a recently described entity which is often misdiagnosed as chronic lymphocytic leukemia or follicular center cell lymphoma. The significance of timely, accurate diagnosis of MCL is of extreme importance since it has a more aggressive clinical course than CLL or FCC. Peripheral blood specimens of admitted patients are routinely scanned by an automated complete blood count (CBC) device. If the CBC flags a specimen as suspicious, the cellular materials are reviewed by a medical technologist. Based upon a subjective morphologic inspection of the constituent cells, a determination is made as to whether the cells are benign. If atypical cells are detected, the slide is forwarded to a pathologist for review. The potential for missed abnormal cells in this screening process is significant. The system that we have developed enables individuals to make decisions based upon the collective “digital experience” of past consensus-graded cases and objective, reproducible image metrics which may be too subtle for detection by unassisted, visual inspection.

Table I and Table II show that human performance is similar to that of the computer-based system for FCC and NORMAL cases, but in terms of the probability of correct decision (the bolded diagonals) and probability of false negatives (the NORMAL column), human performance is worse than that of the machine for CLL and MCL cases. The data also suggest that, for both human observers and for the computer-based system, classifying CLL and MCL cells is relatively more dif-

ficult than classifying FCC cells. While the statistics presented here suggest that the clinical decision support system can outperform human observers, it must be stressed that in an actual clinical setting human experts utilize a tremendous amount of ancillary patient data in conjunction with the clinical cues which are inferred from the pathology specimens. It is not standard practice for these individuals to base a diagnosis on a single cell.

In the past few years, several telepathology systems that feature remote control of a robotic microscope have been developed [26]. These systems are typically passive, however, in that they focus on remote access and the associated image transfer technology. The system described here offers a fully automated indexing and database management interface for recording salient visual and clinical information and provides clinical decision support for screening for hematologic malignancies and for computer-assisted diagnosis. With the addition of temporal data, the system might be used as a tool for staging, disease management, and clinical outcome studies.

V. FUTURE WORK

In order to facilitate the expansion of ground truth databases, a two-phase (immunofluorescence and light) imaging methodology for *in situ* immunophenotyping, cell selection, and digitization is being developed. One of the most important improvements that will be made to the system is the modification of the decision support module in order to allow “open set” inputs from

digitized specimens. This will require the construction of rejection regions for cells which do not belong to the predefined disease class sets. For example, in the prototype problem domain, when a digital specimen containing the spectrum of normal red blood cells, platelettes, etc., is presented, the system should automatically reject any nonsalient components. The next-generation system will feature an automatic mode in which the entire specimen can be systematically scanned by the robotic microscope. In the automated mode, the system will record the spatial coordinates of each cell that exhibits a suspicious spectral and spatial profile. A summary of the cellular composition of the specimen and statistically most likely diagnosis will then be reported to the technician. The system will allow for systematic review of any cells that were categorized as malignant. The expanded database and next-generation platform will be used for iterative experimentation in order to determine the preferred properties of the query that maximize the accuracy of differential diagnosis, and to establish objective criteria for improved screening. A long-term goal for this research is to explore the potential use of the computer-based decision support strategy in a broader range of biomedical applications.

ACKNOWLEDGMENT

The authors would like to thank M. Osman for her help in preparing specimens and for her professional advice. They also wish to thank W. Chen, G. Pullen, J. Salim, Dr. K. Briggs, and Dr. E. Fox for their contributions to the project.

REFERENCES

- [1] J. Garcia-Conde and F. Cabanillas, "Mantle cell lymphoma: A lymphoproliferative disorder associated with aberrant function of the cell cycle," *Leukemia*, vol. 10, pp. s78-s83, 1996.
- [2] G. Vadlamudi, "Leukemic phase of mantle cell lymphoma: Two case reports and review of the literature," *Arch. Pathol. Lab. Med.*, vol. 120, pp. 35-40, 1996.
- [3] Y. Yatabe, "Clinicopathologic study of PRAD1/Cyclin D1 overexpressing lymphoma with special reference to mantle cell lymphoma—A distinct molecular entity," *Amer. J. Surg. Pathol.*, vol. 20, no. 9, pp. 1110-1122, 1996.
- [4] S. Zink and C. C. Jaffe, "Medical imaging databases: A national institutes of health workshop," *Investigative Radiol.*, vol. 28, no. 4, pp. 366-372, 1993.
- [5] J. Chan and P. M. Banks, "A revised European-American classification of lymphoid neoplasms proposed by the international lymphoma study group—A summary version," *Amer. J. Clin. Pathol.*, vol. 103, no. 5, pp. 543-560, 1995.
- [6] C. Rozman and E. Montserrat, "Chronic lymphocytic leukemia," *N.E.J.M.*, vol. 333, no. 16, pp. 1052-1057, 1995.
- [7] M. N. Kilo and D. M. Dorfman, "The utility of flow cytometric immunophenotypic analysis in the distinction of small lymphocytic lymphoma/chronic lymphocytic leukemia from mantle cell lymphoma," *Amer. J. Clin. Pathol.*, vol. 105, pp. 451-457, 1996.
- [8] C. H. Geisler and J. K. Larsen, "Prognostic importance of flow cytometric immunophenotyping of 540 consecutive patients with B-cell chronic lymphocytic leukemia," *Blood*, vol. 78, no. 7, pp. 1795-1802, 1991.
- [9] M. Genesereth and N. Nilson, *Logical Foundations of Artificial Intelligence*. Palo Alto, CA: Morgan Kaufman, 1988, pp. 19-45.
- [10] J. M. Bennett, D. Catovsky, and M. T. Daniel, "Proposals for the classification of acute leukemias," *Br. J. Haematol.*, vol. 33, pp. 451-458, 1976.
- [11] D. R. Head, R. A. Savage, and L. Cerozo, "Reproducibility of the French-American-British classification of acute leukemias: The southwest oncology group experience," *Amer. J. Hematol.*, vol. 18, pp. 47-57, 1985.

- [12] H. Harms, H. M. Aus, M. Haucke, and U. Gunzer, "Segmentation of a stained blood images measured at high scanning density with high magnification and high numerical aperture optics," *Cytometry*, vol. 7, pp. 522-531, 1986.
- [13] I. Bauman, R. Nenninger, H. Harms, H. Zwierzina, K. Wilms, A. C. Feller, V. T. Meulen, and H. K. Muller-Hermelink, "Image analysis detects lineage—Specific morphologic markers in leukemic blast cells," *Amer. J. Clin. Pathol.*, vol. 105, no. 1, pp. 23-30, 1995.
- [14] D. J. Comaniciu and P. Meer, "Distribution free decomposition of multivariate data," *Pattern Anal. Applicat.*, vol. 2, pp. 22-30, 1999.
- [15] D. G. Kendall, "A survey of the statistical theory of shape," *Statistical Science*, vol. 4, pp. 87-120, 1994.
- [16] M. K. Hu, "Visual pattern recognition by moment invariants," *IRE Trans. Inform. Theory Inform. Technol.*, vol. 8, pp. 179-187, 1962.
- [17] I. L. Dryden and K. V. Mardia, *Statistical Shape Analysis*. West Sussex, U.K.: Wiley, 1998, pp. 251-278.
- [18] A. Khotanzad and Y. H. Hong, "Invariant image recognition by Zernike moments," *IEEE Trans. Pattern Anal. Machine Intell.*, vol. 12, pp. 489-497, 1990.
- [19] —, "Rotation invariant image recognition using features selected via a systematic method," *Pattern Recognit.*, vol. 23, pp. 1089-1101, 1990.
- [20] H. T. K. Seppanen and M. Pietikainen, "An experimental comparison of autoregressive and fourier-based descriptors in 2D classification," *IEEE Trans. Pattern Anal. Machine Intell.*, vol. 17, pp. 201-207, 1995.
- [21] F. P. Kuhl and C. R. Giardina, "Elliptic Fourier features of a closed contour," *Computer Graph. Image Process.*, vol. 18, pp. 236-258, 1982.
- [22] J. Mao and A. K. Jain, "Texture classification and segmentation using multiresolution simultaneous autoregressive models," *Pattern Recognit.*, vol. 25, pp. 173-188, 1992.
- [23] W. H. Press, S. A. Teukolsky, W. T. Vetterling, and B. P. Flannery, *Numerical Recipes in C*, 2nd ed. Cambridge, U.K.: University Press, 1992.
- [24] B. Efron and R. Tibshirani, *An Introduction to the Bootstrap*. New York, NY: Chapman and Hall, 1993.
- [25] W. H. Press, S. A. Teukolsky, W. T. Vetterling, and B. P. Flannery, *Numerical Recipes in C*, 2nd ed. Cambridge, U.K.: University Press, 1992.
- [26] G. J. Grimes, "Remote microscopy for hi-res real-time interactive pathology," *Advanced Imaging*, vol. 12, no. 7, pp. 12-16, 1998.

David J. Foran (S'89-M'91) received the B.S. degree from Rutgers University, New Brunswick, NJ, in 1983 and the Ph.D. degree in biomedical engineering from the University of Medicine and Dentistry of New Jersey (UMDNJ) & Rutgers University, Piscataway, NJ, in 1992.

He served as a Physics Instructor at New Jersey Institute of Technology, Newark, NJ, from 1984 to 1985 and worked as a Junior Scientist at Johnson & Johnson Research, Inc., North Brunswick, NJ, from 1986 to 1988. He received one year of post-doctoral training at the Department of Biochemistry at UMDNJ-Robert Wood Johnson Medical School (RWJMS) in 1993. He joined the faculty at RWJMS in 1994 where he is currently an Assistant Professor of Pathology & Radiology and the Director of the interdepartmental Center for Biomedical Imaging & Informatics. He is a member of the graduate faculty in the Program in Computational Molecular Biology and Genetics and is a Research Assistant Professor at the Center for Advanced Information Processing, both at Rutgers University. His research interests include quantitative, biomedical imaging, computer-assisted diagnosis, and medical informatics.

Dorin Comaniciu (S'95-M'99) received the Dipl. Engr. and D.Sc. degrees in electronics from the Polytechnic University of Bucharest, Romania, in 1988 and 1995, respectively, and the Ph.D. degree in electrical engineering from Rutgers University, New Brunswick, NJ, in 1999.

From 1988 to 1990, he was with ICE Felix Computers, Romania. Between 1991 and 1995, he was a Teaching Assistant at the Polytechnic University of Bucharest and, between 1996 and 1999, he was with the Center for Advanced Information Processing, Rutgers University. He held research appointments in Germany and France. Since 1999, he has been with Siemens Corporate Research, Princeton, NJ. His research interests include robust methods for computer vision, nonparametric analysis, content-based image/video retrieval, and data compression.

Peter Meer (S'84–M'86–SM'95) received the Dipl. Engn. degree from Bucharest Polytechnic Institute, Bucharest, Romania, in 1971, and the D.Sc. degree from the Technion, Israel Institute of Technology, Haifa, in 1986, both in electrical engineering.

From 1971 to 1979, he was with the Computer Research Institute, Cluj, Romania, working on the research and development of digital hardware. Between 1986 and 1990, he was an Assistant Research Scientist at the Center for Automation Research, University of Maryland, College Park. In 1991, he joined the Department of Electrical and Computer Engineering, Rutgers, University, Piscataway, NJ, and is currently an Associate Professor. He has held visiting appointments in Japan, Korea, Sweden, Israel, and France and was on the organizing committees of several international workshops and conferences. His research interest is in the application of modern statistical methods to image understanding problems.

Dr. Meer is an Associate Editor of the IEEE TRANSACTIONS ON PATTERN ANALYSIS AND MACHINE INTELLIGENCE and is a member of the Editorial Board of the journal *Pattern Recognition*.

Lauri A. Goodell received the B.A. degree from Rutgers University, New Brunswick, NJ, and the M.D. degree from the University of Medicine and Dentistry of New Jersey–Robert Wood Johnson Medical School.

She served as a Pathology Resident at the University of Arizona Health Sciences Hospital, Tucson. At Robert Wood Johnson University Hospital, she served as Chief Resident from 1994 to 1995. She was a Surgical Pathology/Cytopathology Fellow from 1995 to 1996 and a Hematopathology Fellow from 1996 to 1997. She joined the faculty at Robert Wood Johnson Medical School in 1997 and currently serves as an Assistant Professor. Her research currently focuses on immunologic and molecular probes for leukemias and lymphomas.